UC Davis
UC Davis Previously Published Works

Title

LET-99 functions in the astral furrowing pathway, where it is required for myosin enrichment in the contractile ring

Permalink

Journal

ISSN

Authors

Price, Kari L
Rose, Lesilee S

Publication Date

DOI

Peer reviewed

LET-99 functions in the astral furrowing pathway, where it is required for myosin enrichment in the contractile ring

Kari L. Price and Lesilee S. Rose*
Department of Molecular and Cellular Biology and Biochemistry, Molecular, Cellular and Developmental Biology Graduate Program, University of California, Davis, Davis, CA 95616

ABSTRACT The anaphase spindle determines the position of the cytokinesis furrow, such that the contractile ring assembles in an equatorial zone between the two spindle poles. Contractile ring formation is mediated by RhoA activation at the equator by the centralspindlin complex and midzone microtubules. Astral microtubules also inhibit RhoA accumulation at the poles. In the *Caenorhabditis elegans* one-cell embryo, the astral microtubule–dependent pathway requires anillin, NOP-1, and LET-99. LET-99 is well characterized for generating the asymmetric cortical localization of the Gα-dependent force-generating complex that positions the spindle during asymmetric division. However, whether the role of LET-99 in cytokinesis is specific to asymmetric division and whether it acts through Gα to promote furrowing are unclear. Here we show that LET-99 contributes to furrowing in both asymmetrically and symmetrically dividing cells, independent of its function in spindle positioning and Gα regulation. LET-99 acts in a pathway parallel to anillin and is required for myosin enrichment into the contractile ring. These and other results suggest a positive feedback model in which LET-99 localizes to the presumptive cleavage furrow in response to the spindle and myosin. Once positioned there, LET-99 enhances myosin accumulation to promote furrowing in both symmetrically and asymmetrically dividing cells.

INTRODUCTION

During cytokinesis, the final step in cell division, the cortical cytoskeleton undergoes a dramatic reorganization from a uniform meshwork of actin and myosin to a contractile ring that divides the cell. The position of the contractile ring, and ultimately the site of division, is determined by the position of the anaphase spindle (Rappaport, 1996). Cytokinesis is spatially and temporally coupled to chromosome segregation, as constriction of the contractile ring occurs in response to signals from the anaphase spindle; this ensures that each resulting daughter cell receives the proper

cytoplasmic constituents and a copy of each of the segregating chromosomes (Glotzer, 2004; D'Avino *et al.*, 2005; Eggert *et al.*, 2006). Two populations of microtubules contribute to these furrowing signals: the long astral microtubules that emanate from centrosomes to reach the cortex and the nonkinetochore, overlapping, antiparallel microtubules that form the central spindle or midzone. Signals from both populations of microtubules localize and activate the small GTPase RhoA at the equator before the onset of furrowing (Maddox and Oegema, 2003; Glotzer, 2005; Eggert *et al.*, 2006). When bound to GTP, RhoA activates formins and Rho kinase, resulting in actin polymerization, as well as regulatory myosin light chain phosphorylation (Pollard, 2010; Green *et al.*, 2012). Activated myosin assembles into minifilaments and through its motor activity cross-links and slides unbranched actin filaments relative to one another, providing some of the force to initiate furrow formation and drive membrane ingression (Piekny *et al.*, 2005). In addition, myosin-independent cross-linking of actin coupled with actin depolymerization provides contractile force for constriction (Zumdieck *et al.*, 2007; Carvalho *et al.*, 2009). As constriction continues and the membrane ingresses extensively, a

midbody structure forms to stabilize the furrow until abscission occurs to complete cytokinesis.

The components that constitute the central spindle signal are well characterized. The conserved heterotetrameric centralspindlin complex contains the kinesin subunit ZEN-4 (MKLP1 in vertebrates) and the GTPase-activating subunit CYK-4 (MGCRacGap). This complex localizes to midzone microtubules and at the membrane of the presumptive cleavage furrow and is required for the recruitment of the RhoGEF ECT-2, which activates RhoA to promote furrowing (Raich *et al.*, 1998; Verbrugghe and White, 2004; Basant *et al.*, 2015). In contrast, dynamic astral microtubules inhibit the accumulation of RhoA and other furrowing components at the polar cortex, biasing recruitment of these components between the asters in an equatorial band (Werner *et al.*, 2007; Chen *et al.*, 2008; Foe and von Dassow, 2008; Zhou and Wang, 2008; Lewellyn *et al.*, 2010).

Different cell types display different requirements for the central spindle and astral microtubules in furrowing. Studies in *Drosophila* and mammalian cultured cells show that furrow initiation signals from the central spindle appear to be essential, as there is a complete loss of furrowing in cells with compromised central spindles/ centralspindlin (Cao and Wang, 1996; Wheatley and Wang, 1996; Adams *et al.*, 1998). In contrast, furrowing in the *Caenorhabditis elegans* one-cell embryo, grasshopper spermatocytes, cultured HeLa and epithelial cells, and early frog and sea urchin embryos can initiate even when depleted of the centralspindlin complex or central spindle microtubules, although often the furrow regresses and cytokinesis fails (Jantsch-Plunger *et al.*, 2000; Alsop and Zhang, 2004; Murthy and Wadsworth, 2008; Piekny and Glotzer, 2008; von Dassow, 2009).

In early *C. elegans,* frog, and sea urchin embryos, furrowing defects caused by loss of centralspindlin or central spindle microtubules are enhanced if spindle pole separation is attenuated (Dechant and Glotzer, 2003; von Dassow, 2009; Lewellyn *et al.*, 2010). Further evidence for distinct centralspindlin and astral microtubule pathways comes from laser ablation and genetic studies that spatially separate the two pathways, resulting in formation of multiple furrows in response to their respective furrow-inducing signal (Bringmann and Hyman, 2005; Werner *et al.*, 2007). For example, depletion of the microtubule polymerase ZYG-9 causes formation of a smaller posterior spindle in the *C. elegans* one-cell embryo, which results in two distinct furrows. One furrow forms in the posterior, adjacent to the spindle midzone, and requires centralspindlin (ZEN-4/CYK-4) activity (Loria *et al.*, 2012). Concurrently, in response to inhibition from the posterior astral microtubules, myosin accumulates in the anterior half of the embryo and assembles an ectopic, central spindle–independent furrow (Werner *et al.*, 2007).

The molecular mechanism for the astral pathway is unclear, but components required for furrowing in this pathway have been identified by their enhancement of the furrowing defects of *centralspindlin* mutants (Tse *et al.*, 2011, 2012). NOP-1 was first described for its role in pseudocleavage in *C. elegans,* which is the formation of an aster-directed furrow in response to myosin flows during polarization of the one-cell embryo. *nop-1* mutant embryos exhibit markedly reduced myosin flows and fail to form the pseudocleavage furrow but ultimately polarize via redundant mechanisms. During cytokinesis, NOP-1 is required to promote RhoA activation in the astral pathway, in parallel to the ZEN-4/CYK-4 centralspindlin pathway (Rose *et al.*, 1995; Morton *et al.*, 2012; Tse *et al.*, 2012). The highly conserved anillin protein ANI-1 is required to organize cortical myosin into discrete patches during polarization and at anaphase onset in *C. elegans* (Maddox *et al.*, 2005; Tse *et al.*, 2011). The interactions of anillin with cytokinesis components, including

formins, nonmuscle myosin II, RhoA, ECT-2, and septins in other systems, suggest that it acts as a general cytoskeletal scaffold (Piekny and Maddox, 2010). In the one-cell *C. elegans* embryo, ANI-1 coordinates cortical actomyosin organization downstream of both the central spindle and astral furrowing signals (Tse *et al.*, 2012). However, examination of ANI-1 function in furrow formation suggests that the astral pathway is more sensitive to loss of ANI-1 because RNA interference (RNAi) of *ani-1* enhances the furrowing defects of *centralspindlin* mutants but not *nop-1* mutants (Werner and Glotzer, 2008; Tse *et al.*, 2011). Similarly, in HeLa cells, depletion of anillin in combination with depletion of centralspindlin results in a complete loss of furrowing (Piekny and Glotzer, 2008). Like NOP-1, ANI-1 is also required for pseudocleavage in *C. elegans,* consistent with a role in actomyosin contractility that is inhibited by astral microtubules (Maddox *et al.*, 2005).

To identify other components of the astral microtubule pathway in *C. elegans*, an enhancer screen for furrowing defects was performed in *spd-1* embryos, which lack central spindle microtubules. This screen identified the spindle-positioning regulators LET-99, Gα, and GPR-1/2 as additional candidates for astral pathway components (Bringmann *et al.*, 2007). The Gα/GPR-1/2/LIN-5 (Gα/LGN/NuMA and Gα/Pins/Mud in vertebrates and *Drosophila,* respectively) complex recruits dynein to generate forces that position the spindle in many cell types, including the first asymmetric division of the *C. elegans* embryo (Rose and Gonczy, 2014). LET-99 is a DEP domain– containing protein (domain found in Disheveled, Egl-10, and Plekstrin) that localizes to the cell cortex and is enriched in a posterior-lateral band downstream of polarity establishment in *C. elegans* (Tsou *et al.*, 2002; Wu and Rose, 2007). LET-99 inhibits the localization of GPR-1/2 and LIN-5 from the posterior-lateral cortex, resulting in asymmetric GPR/LIN-5 localization and thus asymmetric forces. In *let-99* mutant one-cell embryos, GPR-1/2 and LIN-5 are uniformly high, and the nuclear–centrosome complex exhibits excessive nuclear rocking and spindle-positioning defects (Rose and Kemphues, 1998; Tsou *et al.*, 2002, 2003; Krueger *et al.*, 2010). Spindle elongation is also compromised in *let-99* mutants, raising the possibility that the failure of furrowing in *let-99;spd-1* embryos is an indirect effect of the need for spindle pole separation in the astral pathway. However, studies of embryos with spatially separated furrows induced by a posterior spindle showed that *let-99(RNAi)* embryos also exhibited a reduction in anterior furrow ingression (Werner *et al.*, 2007). Thus LET-99 appears to be a bona fide component of the astral pathway. Depletion of LET-99 also resulted in a reduction in residence time of cortical nonmuscle myosin (NMY-2) foci at anaphase in embryos with a posterior spindle, and abnormal myosin organization in the contractile ring at cytokinesis was observed in *let-99* embryos with a bipolar spindle (Bringmann *et al.*, 2007; Werner *et al.*, 2007). However, the relationship between LET-99 and other components of the astral inhibition pathway has not been determined.

During prophase, LET-99 localizes to the cortex and becomes asymmetric in response to the PAR polarity proteins: LET-99 is excluded from the anterior by PAR-3 and from the posterior by PAR-1 and PAR-5, forming a band (Tsou *et al.*, 2002; Wu and Rose, 2007; Wu *et al.*, 2016). LET-99 cortical band localization persists through anaphase, and LET-99 is present in the ingressing cleavage furrow. This anaphase localization is PAR independent. For example, in *par-3* mutants, although LET-99 is initially uniformly enriched at the cortex, a broad-banded pattern is present in anaphase and is symmetrically positioned like the spindle (Tsou *et al.*, 2002; Wu and Rose, 2007). Further, mechanical displacement of the spindle revealed that LET-99 localization changes in response to the new position of the spindle at anaphase but not before metaphase

(Bringmann et al., 2007). However, whether LET-99 localization to the equatorial cortex over the spindle is directed by the astral or central spindle microtubules is not known.

During late anaphase in wild-type embryos, GPR-1/2 are excluded from the region of the LET-99 band and thus the furrow, but in let-99 embryos, GPR localizes to the furrow (Bringmann et al., 2007; Panbianco et al., 2008; Park and Rose, 2008). Thus LET-99 has an antagonistic relationship with GPR-1/2 at this stage, as in spindle positioning. Gα was reported to be positively required for normal LET-99 localization at cytokinesis. In embryos depleted of the partially redundant Gα subunits GOA-1 and GPA-16, the LET-99 band was more posterior than in wild type (Bringmann et al., 2007). These observations, coupled with the enhancement of furrowing defects by loss of GPR-1/2 and Gα in a centralspindlin-defective background, raise the possibility that LET-99 functions to promote furrowing through Gα or GPR-1/2 (Bringmann et al., 2007). However, the role of all of these proteins in cytokinesis is potentially complicated by spindle elongation and positioning defects in the mutants. Sufficient spindle pole elongation appears to be critical for cleavage furrow specification in the absence of a central spindle in several cell types (Dechant and Glotzer, 2003; von Dassow, 2009; Lewellyn et al., 2010). Thus the failure of Gα;zen-4 and gpr-1/2;zen-4 embryos to furrow or promote myosin localization at the equator has been interpreted as a consequence of their spindle elongation defects in some studies (Dechant and Glotzer, 2003; Werner et al., 2007). At the same time, other studies indicate that spindle length does not always correlate with defective furrowing in Gα and GPR-1/2 mutants (Verbrugghe and White, 2004; Bringmann et al., 2007). Thus whether Gα plays a direct role in furrowing or LET-99 localization is unclear. Further, it is not known whether the effects of LET-99 or Gα on cytokinesis are specific to asymmetrically dividing cells. The one-cell embryo has an inherent asymmetry of actomyosin at the anterior before cytokinesis, and thus there may be special requirements for reorganization into the contractile ring, as shown recently for the PAR proteins (Jordan et al., 2016).

Here we show that loss of LET-99 in zen-4 (centralspindlin-defective) embryos results in furrowing defects in the symmetrically dividing AB cell of the two-cell embryo, as well as in the one-cell embryo, and that furrowing defects are independent of spindle positioning and elongation. Although LET-99 is uniform in the AB cell initially, LET-99 localizes to the equator just before cytokinesis, and neither this localization nor furrowing in the AB cell requires Gα. Genetic analysis places LET-99 in a pathway with NOP-1, acting in parallel to anillin to promote furrowing. Of interest, LET-99 localization at anaphase in the one-cell embryo responds to astral microtubules but also to the centralspindlin pathway. LET-99 localization requires NMY-2, but at the same time NMY-2 fails to enrich into a contractile band when both the centralspindlin pathway and LET-99 are absent. Our findings suggest a feedback mechanism in which the mitotic spindle refines LET-99 localization to align with the furrow, possibly via myosin movement, where LET-99 is then required for further myosin accumulation into a contractile ring.

RESULTS

LET-99 is required for furrowing during both asymmetric and symmetric division

Previous studies showed that the spindle elongation defect exhibited by let-99 embryos is not the sole cause of furrow failure in let-99 embryos without a central spindle, because a let-99 allele was identified that reduced spindle elongation without affecting furrowing (Bringmann et al., 2007). Nonetheless, the furrowing defects of let-99;centralspindlin mutants are highly variable, raising the possibility

that spindle elongation defects contribute to the phenotype (Bringmann et al., 2007; Pacquelet et al., 2015). In addition, the correlation between altered spindle position and furrowing in let-99 embryos has not been analyzed; in let-99 mutants, alignment of the spindle onto the anterior-posterior (AP) axis at the one-cell stage is often late (Supplemental Movies S1 and S2), and a misoriented posterior spindle pole may not stimulate furrowing to the same degree as in wild type. Thus, to examine more carefully whether spindle-positioning defects exacerbate the let-99 phenotype and to provide a baseline for mutant comparisons, we quantified the extent of furrow ingression in one-cell embryos, as well as the distance between the two spindle poles, the position of the posterior spindle pole, and the angle of the spindle at furrowing onset. We used the let-99(dd17) null mutant and RNAi of zen-4 to remove centralspindlin function, as well as zen-4(or153ts)—hereafter referred to as zen-4(ts)—one-cell embryos depleted of LET-99 via RNAi. This temperature-sensitive allele of zen-4 disrupts the interaction between ZEN-4 and CYK-4 that is required for centralspindlin function (Severson et al., 2000; Pavicic-Kaltenbrunner et al., 2007; Canman et al., 2008). Loss of ZEN-4 also prevents central spindle assembly and should therefore rescue defects in spindle elongation caused by loss of LET-99 that might otherwise compromise furrow formation. Only embryos in which RNAi produced the published loss of function phenotypes (see Materials and Methods) were analyzed.

The extent of furrow ingression was measured by the ratio of the distance between opposing membranes at maximum ingression to the widest part of the embryo in the same frame (Figure 1A); embryos were followed until the beginning of the two-cell stage as evidenced by nuclear reformation. Shallow, transient cortical indentations without a sustained furrow were scored as a complete failure of ingression, as described previously (Bringmann et al., 2007). In zen-4(RNAi) embryos, we observed an average furrow ingression of 50.71 ± 3.21% embryo width (n = 10) and an average spindle elongation of 25.4 ± 0.5 μm (Figure 1 and Supplemental Figure S1B, respectively and Supplemental Movie S3). In let-99(dd17);zen-4(RNAi) embryos, furrows ingressed to an average of 8.16 ± 0.99% embryo width (n = 18; Figure 1B). In the latter embryos, two of 13 embryos completely failed to furrow, and numerous small cortical indentations were observed (Supplemental Movie S4). Similar furrowing defects were observed in zen-4(ts);let-99(RNAi) embryos compared with zen-4(RNAi);let-99(dd17)embryos (Supplemental Figure S1A). Spindle poles separated to greater distances in let-99(dd17);zen-4(RNAi) double mutants than in let-99 single mutants (20.3 ± 0.2 and 15.9 ± 0.3 μm, respectively), comparable to wild-type spindle pole separation (21.5 ± 0.5 μm; Supplemental Figure S1B). Further, when spindle pole elongation was plotted relative to furrow ingression, we failed to detect a correlation (p = 0.48; Figure 1C). Similarly, although the final position of the posterior spindle pole is slightly more anterior in let-99(dd17) than in wild type, zen-4(RNAi) rescues the defects caused by let-99 to within wild-type values (Supplemental Figure S1, C and D). When the position of the posterior spindle pole in let-99(dd17);zen-4(RNAi) embryos was plotted relative to furrow ingression, we found no correlation between more posteriorly positioned spindle poles and better furrow ingression (p = 0.52; Figure 1D), and there was also no correlation between spindle angle in these embryos relative to furrow ingression (p = 0.12; Supplemental Figure S1F). These results suggest that the enhancement of the furrowing defect produced by let-99 in the zen-4 background is due largely to the role of LET-99 in cytokinesis and not its spindle-positioning phenotype.

To determine the contribution of LET-99 to furrowing in a symmetrically dividing cell, we examined division of the AB cell
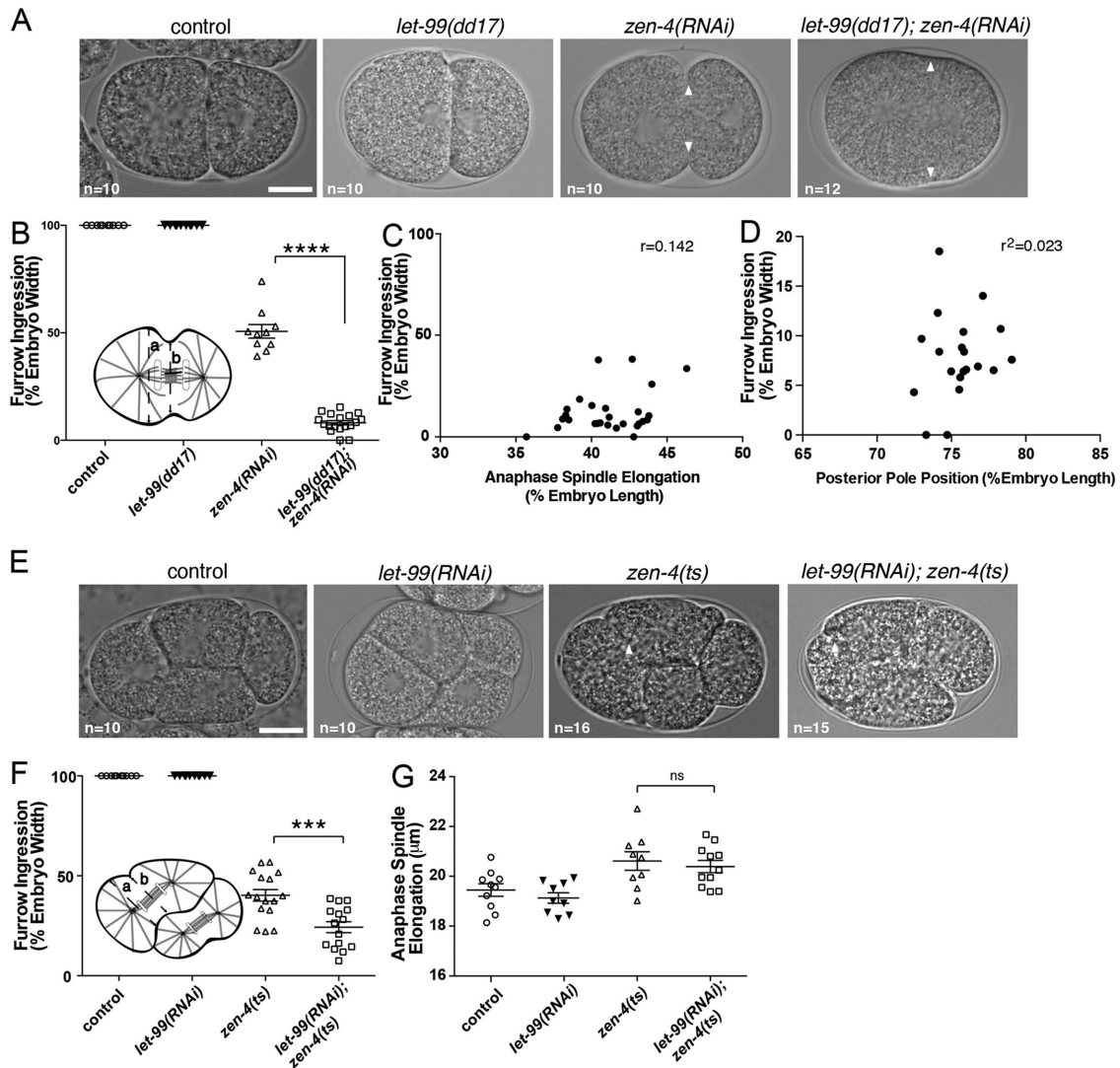
FIGURE 1: LET-99 promotes furrowing in asymmetric and nonasymmetric divisions. (A) Bright-field/DIC images from time-lapse microscopy showing either completion of cytokinesis or the point of maximum furrow ingression (white arrowheads). (B) Quantification of maximum ingression in the one-cell embryo, as shown in the schematic, where b represents the distance between opposing sides of the embryo at maximum furrow ingression, and a represents the widest part of the embryo at the same time point; % ingression = $b/a \times 100$. (C) Correlation of furrow ingression and anaphase spindle length in *let-99(dd17);zen-4(RNAi)* and *let-99(RNAi);zen-4(ts)* embryos (Spearman correlation analysis, $r = 0.142$, $p = 0.47$, ns). (D) Correlation of furrow ingression and position of the posterior spindle pole at anaphase in *let-99(dd17);zen-4(RNAi)* and *let-99(RNAi);zen-4(ts)* embryos (Pearson correlation analysis, $r^2 = 0.023$, $p = 0.51$, ns). (E) Bright-field images from time-lapse microscopy of division in the AB cell of two-cell embryos. Arrowhead marks the membrane at maximum furrow ingression. (F) Quantification of furrow ingression in the AB cell reported as percentage of AB cell width measured as shown in the schematic. (G) Quantification of spindle elongation in AB cell at anaphase. Scale bars, 10 μm. Anterior is to the left in this and all figures. Error bars represent ± SEM. ns = $p \geq 0.05$; ***$p < 0.001$; ****$p < 0.0001$.

(Figure 1E). In the AB cell, there are no asymmetric spindle-positioning events, allowing us to address a role for LET-99 in furrowing specifically. The extent of ingression in the AB cell was measured as a ratio of the opposing membranes at maximum furrow ingression to the widest part of the AB cell in the same frame (Figure 1F). We used *zen-4(ts)* embryos to circumvent the requirement of ZEN-4 in the first embryonic cytokinesis. In *zen-4(ts)* embryos shifted to the nonpermissive temperature after completion of the first embryonic cytokinesis, furrows ingressed to an average of 40.23 ± 2.91% AB cell width (Figure 1F). In *let-99(RNAi);zen-4(ts)* embryos, furrows ingressed an average of 24.28 ± 2.73% AB cell width. Spindles in

zen-4(ts) embryos elongated slightly greater than in controls (20.61 ± 0.4 vs. 19.45 ± 0.3 μm; Figure 1G). However, AB spindle elongation was not affected in *let-99(RNAi)* embryos (19.06 ± 0.2 μm), in contrast to the situation in the one-cell embryo. Thus the decrease in furrowing observed in the AB cell of *let-99(RNAi);zen-4(ts)* embryos cannot be explained by poor spindle elongation. Together with the observations of one-cell embryos, these results indicate that the defects in furrowing observed after loss of LET-99 are independent of spindle elongation and position and further show that the role of LET-99 in furrowing is not specific to asymmetrically dividing cells.
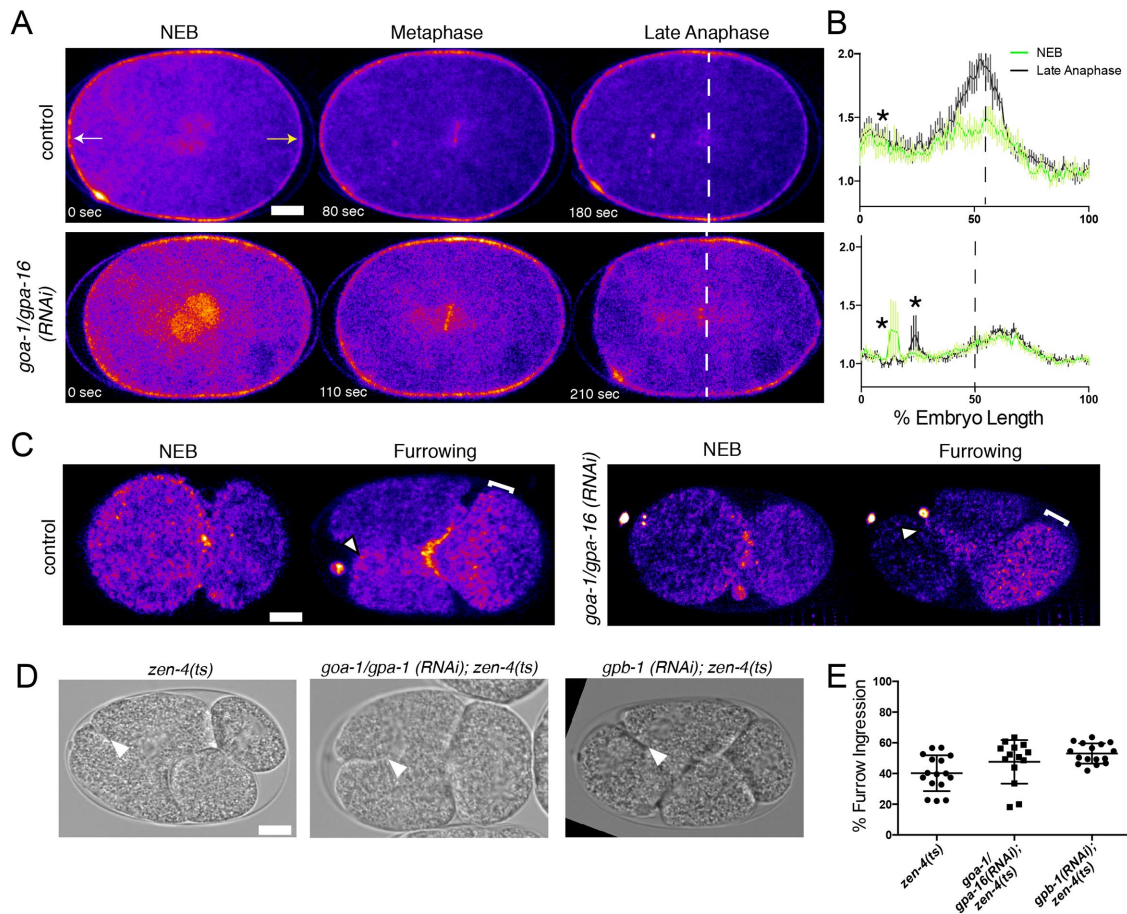
FIGURE 2: Gα is not directly required for furrowing in the AB cell. (A) Spinning-disk confocal images from time-lapse movies of YFP::LET-99 embryos. Representative embryos; both sides of the embryo cortex were traced from anterior (white arrow) to posterior (yellow arrow) to generate a plot of pixel intensities along the AP axis. (B) Average line scans for all embryos (control *n* = 11; *goa-1/gpa-16(RNAi) n* = 9). NEB and late anaphase are shown with an asterisk marking peaks in signal from the polar body and a dashed line representing the plane of division. (C) YFP::LET-99 or YFP::LET-99; *goa-1/gpa-16(RNAi)* cortical images at NEB and furrowing onset. White arrowheads mark the YFP::LET-99 at the furrow in the AB cell, brackets mark the YFP::LET-99 band in the P1 cell. (D) Bright-field images to show the maximum extent of furrow ingression. (E) Furrow ingression in the AB cell is quantified as described in Figure 1. Images in A and C are pseudocolored with Fire LUT such that the highest pixel values are pink/white and the lowest pixel values are blue/purple. Scale bars, 10 μm. Error bars represent ± SEM.

In the one-cell embryo, LET-99 is localized by the PAR proteins in a posterior lateral band pattern at the cortex (Figure 2, A and B). This band aligns with the furrow at cytokinesis, and its anaphase position is influenced by spindle position (Tsou *et al.*, 2002; Bringmann *et al.*, 2007; Wu and Rose, 2007). Because LET-99 enhanced the *zen-4(ts)* furrowing defect in the AB cell, we examined whether LET-99 also localizes to the furrow in this cell. Previous immunolocalization studies showed that LET-99 localization is uniform at the cortex of the AB cell early, but cytokinesis was not examined (Tsou *et al.*, 2002; Bringmann *et al.*, 2007; Wu and Rose, 2007). We therefore used live imaging of a yellow fluorescent protein–tagged LET-99 strain (YFP::LET-99) to follow LET-99 localization throughout the cell cycle. LET-99 is also present in the polar body, which is typically on the anterior pole of the embryo near or at the site of AB furrow ingression when viewed in cross-section. To avoid this polar body signal, we first examined YFP::LET-99 at the two-cell stage from a cortical view using spinning-disk confocal microscopy. Before furrowing onset in the AB cell, YFP::LET-99 was uniform on the AB cortex, but a band of LET-99 was visible in the asymmetrically

dividing P1 cell (Figure 2C). By the time of furrow formation in the AB cell, LET-99 became enriched at the equator of the AB cell (*n* = 9; Figure 2C). A subset of YFP::LET-99 embryos in which the polar body was not at the furrow were filmed in cross-section, which allowed for better correlation to cell cycle. In most embryos, LET-99 was clearly visible at the equator before the onset of furrowing (five of six; in one embryo, localization became apparent at furrowing). This result shows that LET-99 localizes in a band in the AB cell, which does not have asymmetric PAR polarity proteins, consistent with anaphase spindle-dependent localization.

To test whether a bipolar spindle is required for LET-99 localization in the AB cell, we examined localization after depletion of ZYG-1, a key regulator of centrosomal duplication. In *zyg-1(RNAi)* embryos, the first embryonic division occurs normally as two centrioles are deposited from the sperm; however, centrosome duplication fails, resulting in a monopolar spindle in both the AB and P1 cells (O'Connell *et al.*, 2001). In these embryos, LET-99 localization remained uniform throughout the cell cycle in the AB cell, and the cell failed to initiate a furrow (Supplemental Figure S2, A and B;

n = 9). After 300 s with no furrowing, large blebs were seen, similar to those described by Lewellyn *et al.* (2010), presumably due to a failure in aster separation. Taken together, these results suggest that a bipolar spindle-dependent signal localizes LET-99 to the equator at anaphase in the AB cell, as in the one-cell embryo.

Role of LET-99 in cytokinesis is separable from Gα

The partially redundant Gα subunits GOA-1 and GPA-16, and the positive Gα regulators GPR-1/2 were identified in the same screen for aster-directed furrowing components as LET-99 (Bringmann *et al.*, 2007). That study also showed that the peak of mCherry::LET-99 cortical localization did not align with final furrow position in *goa-1;gpa-16(RNAi)* embryos, where the furrow is more centrally positioned than in wild-type embryos. These and other results suggested that Gα may act upstream of LET-99 specifically at cytokinesis (Bringmann *et al.*, 2007). However, whether Gα is also required for the proper positioning of the LET-99 band earlier, when Gα and LET-99 are acting in PAR-directed spindle positioning, was not examined.

To determine more precisely the timing of the requirement for Gα on LET-99 localization, we used live imaging of YFP::LET-99 embryos imaged in cross-section (Figure 2). We traced the embryo cortex from anterior to posterior (0–100% embryo length [EL]) and divided the pixel intensities by the average cytoplasmic signal to generate a cortical/cytoplasmic ratio, which we plotted against EL (Figure 2A shows representative embryos, and Figure 2B shows average plots for each genotype). Although this YFP::LET-99 strain exhibits higher levels of anterior signal of LET-99 in many one-cell embryos compared with published antibody staining (Tsou *et al.*, 2002), a peak of cortical signal was nonetheless visible and positioned in the posterior lateral region (53.8 ± 1.31% EL) by nuclear envelope breakdown (NEB); the peak region of YFP::LET-99 intensity marked the ingressing furrow at cytokinesis (53.8 ± 0.87% EL, *n* = 11). We found that although the overall cortical levels of YFP::LET-99 were slightly lower in *goa-1;gpa-16(RNAi)* embryos at both NEB and anaphase, a clear band of LET-99 was present at both stages. Further, the position of the peak of YFP::LET-99 cortical pixel intensities in *goa-1;gpa-16(RNAi)* embryos was indistinguishable from wild type at NEB (54.0 ± 1.4% EL; Figure 2, A and B). However, the position of the peak of YFP::LET-99 shifted more posteriorly from NEB to anaphase (four of seven embryos) or stayed in the same relative position (three of seven) in *goa-1;gpa-16(RNAi)* embryos; this resulted in a more-posterior peak of LET-99 (58.1 ± 1.89% EL) that did not align with the centrally positioned cleavage furrow (50.1 ± 0.42% EL; Figure 2, A and B). In contrast, in control embryos, the LET-99 peak often adjusted slightly either to the anterior (as in Figure 2A) or to the posterior to match the furrow (five of nine). Together with previous work (Bringmann *et al.*, 2007), these results show that Gα is not necessary for the early PAR-dependent phase of LET-99 localization into a band but is required for alignment of the LET-99 band with the cytokinesis furrow.

Gα was previously shown to play a role in precisely aligning the boundary of the PAR-2 domain with the cytokinesis furrow, a process termed polarity correction; this role appeared to be through the effects of Gα on positioning the spindle toward the posterior, as polarity correction was normal in Gα-depleted embryos that had a posteriorized spindle (Schenk *et al.*, 2010). Thus we postulated that the failure to align the LET-99 band with the furrow in Gα embryos is due to the role of Gα in asymmetric spindle positioning. To test this view further, we examined YFP::LET-99 during the symmetric AB division in *goa-1;gpa-16(RNAi)* embryos. In these embryos, LET-99 was present at the equator and furrow, as seen in the wild-type AB cell (seven of eight embryos; Figure 2C).

To address further the relationship between Gα and LET-99 in the astral pathway, we used two different mutants that separate the astral pathway from the central spindle pathway, *zyg-9* and *zen-4*. To circumvent the requirement of Gα in spindle positioning and elongation, we investigated the effect of loss of Gα on anterior furrow ingression in *zyg-9* embryos. In *zyg-9* embryos, a small spindle assembles in the posterior of the embryo, resulting in the formation of a central spindle–directed furrow at the posterior pole and an ectopic anterior aster-directed furrow (Werner *et al.*, 2007; Loria *et al.*, 2012). The anterior furrow ingressed completely in *goa-1;gpa-16(RNAi); zyg-9(b244)* embryos (11 of 12), just as in *zyg-9* embryos (*n* = 10). In contrast, only one of six *let-99(RNAi);zyg-9(b244)* embryos had anterior furrows that ingressed completely; in the majority of embryos (five of six), the furrow ingressed partially and then regressed, as previously reported (Werner *et al.*, 2007). To test more rigorously the role of Gα, we examined division in the AB blastomere (Figure 2D). In *goa-1;gpa-16(RNAi);zen-4(ts)* two-cell embryos, the extent of furrow ingression was not statistically different from that in *zen-4(ts)* control embryos (Figure 2E; 40.23 ± 2.91 vs. 47.60 ± 3.80%, respectively), in contrast to the defective furrowing in *let-99(RNAi);zen-4(ts)* embryos (Figure 1F). In addition, loss of Gα had no affect on spindle elongation in the AB cell, similar to what we observed in *let-99* embryos: spindle poles elongated to 18.64 ± 0.6 μm in *goa-1;gpa-16(RNAi)* embryos (*n* = 8) compared with 19.25 ± 0.3 μm for wild type (*n* = 10; *p* = 0.41, ns). These data argue against a direct role for Gα in furrow initiation in the astral pathway, but along with previous work (Dechant and Glotzer, 2003; Bringmann *et al.*, 2007; Werner *et al.*, 2007) indicate that spindle elongation and/or posterior spindle pole positioning can influence furrowing during the first asymmetric division.

In *let-99* embryos, excess GPR is present at the cortex (Bringmann *et al.*, 2007), raising the possibility that *let-99* furrowing defects are a secondary consequence of excess GPR. To address this possibility, we carried out RNAi on the Gβ subunit 1 (GPB-1), which is required to sequester Gα in the inactive state. In the absence of GPB-1, Gα is free to interact with and promote GPR-1/2 at the cortex, resulting in increased GPR-1/2 accumulation and excess pulling forces, similar to what is seen in *let-99* embryos (Tsou *et al.*, 2003; Afshar *et al.*, 2008). In *gpb-1(RNAi);zen-4(ts)* embryos, we found an average furrow ingression of 53.03 ± 1.65%, which was no worse than ingression in *zen-4(ts)* control embryos (Figure 2E) and much better than in *let-99(RNAi);zen-4(ts)* (Figure 1F). Therefore we conclude that *let-99* furrowing defects are not a result of overexpression of GPR-1/2. Overall these observations suggest that the role of LET-99 in furrowing is distinct from its role in spindle positioning.
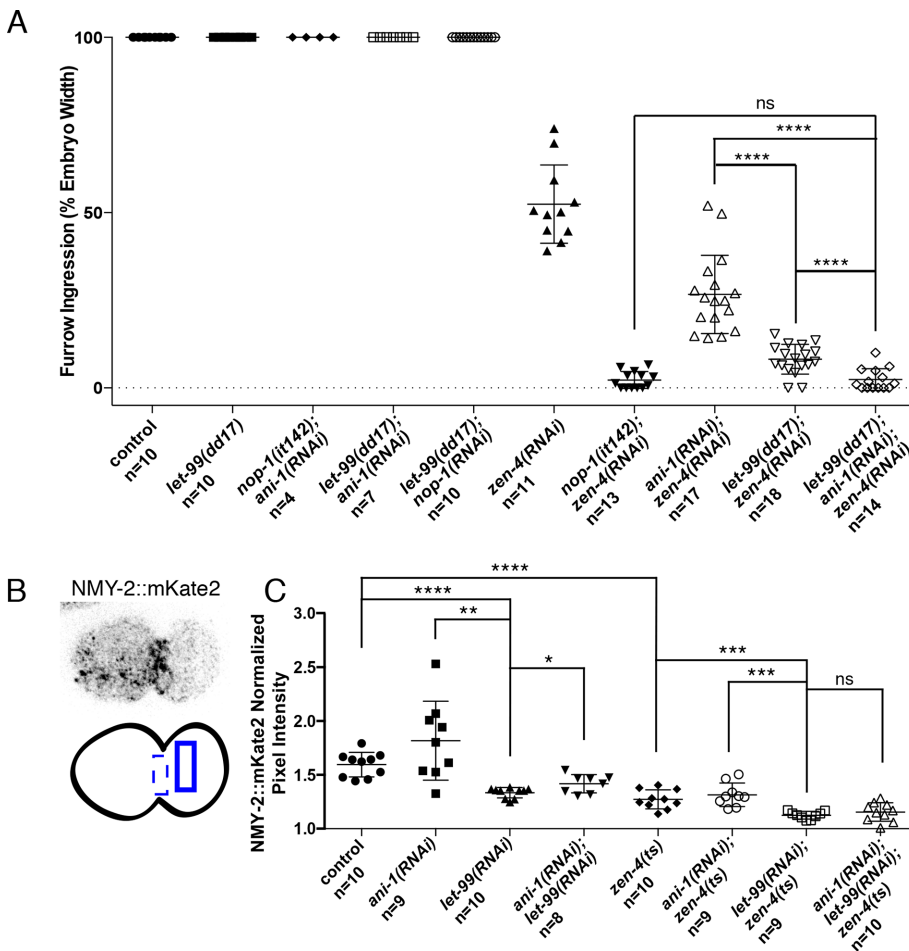
LET-99 acts in parallel to anillin and promotes myosin enrichment in the furrow

To gain more insight into the role of LET-99 in the astral pathway, we carried out double-mutant analyses with *nop-1* and *ani-1*. NOP-1 is believed to be the predominant aster-directed furrowing component; when *nop-1* embryos are depleted of either of the centralspindlin components ZEN-4 or CYK-4, there is a dramatic reduction in the levels of NMY-2 and ANI-1 at the furrow (Tse *et al.*, 2012). Further, *nop-1;centralspindlin*–depleted embryos completely fail to form cleavage furrows, and in *nop-1;zyg-9* embryos, the formation of the anterior astral-dependent furrow is completely blocked (Tse *et al.*, 2012). ANI-1 has been shown genetically to act in the astral pathway: *ani-1;zen-4* embryos show decreased furrowing relative to *zen-4* alone (Werner and Glotzer, 2008), and *ani-1;zyg-9* embryos show a reduction in the anterior but not the posterior furrow (Tse *et al.*, 2011). However *ani-1* and *nop-1;ani-1* embryos undergo complete cytokinesis (Tse *et al.*, 2012).

We measured furrowing in *let-99(dd17);nop-1(RNAi)* and *let-99(dd17);ani-1(RNAi)* one-cell mutant embryos. In both cases, furrowing was complete, just as in *nop-1;ani-1* embryos (Figure 3A), confirming that LET-99 functions in the astral pathway. The furrowing defect of *let-99(dd17);zen-4(RNAi)* embryos is worse than that of *ani-1(RNAi);zen-4(RNAi)* embryos (8.16 ± 0.99 and 26.67 ± 2.70%, respectively) (Supplemental Movie S5), but both are weaker than *nop-1(it142);zen-4(RNAi)* (2.26 ± 0.67%; Figure 3A). However, when we examined furrowing in *let-99(dd17);ani-1(RNAi);zen-4(RNAi)* embryos, we found a greater reduction in furrowing, to 2.38 ± 0.82% embryo width (*n* = 14; Supplemental Movie S6), which is not statistically significant from *nop-1(it142);zen-4(RNAi)*. In addition, 6/14 *let-99(dd17);ani-1(RNAi);zen-4(RNAi)* one-cell anaphase embryos showed aberrant cortical activity with large protrusions, which was not observed in *ani-1(RNAi);zen-4(RNAi)* or *let-99(dd17);zen-4(RNAi)* embryos (Supplemental Movies S4–S6). These results suggest that

LET-99 and ANI-1 act in parallel mechanisms to promote furrowing in the astral pathway.

Like NOP-1, ANI-1 is required for the formation of large myosin patches during both polarization and cytokinesis, but LET-99 is not (Maddox *et al.*, 2005; Bringmann *et al.*, 2007; Werner *et al.*, 2007; Tse *et al.*, 2011, 2012). To determine whether LET-99 is required for other aspects of myosin localization during cytokinesis, we investigated the extent of myosin enrichment by visualization of NMY-2::mKate2 in embryos RNAi-depleted of *let-99, ani-1,* or both. Cortical images of live embryos were taken, and the mean pixel intensity of a 1200-pixel^2 region of interest at the furrow was measured at 100 s after anaphase onset, which corresponds to just after furrow initiation in wild type; values were normalized to a cortical region outside the furrow (Figure 3B). In control embryos expressing NMY-2::mKate2, we found an average cortical-to-cytoplasmic ratio of 1.59 ± 0.032, with myosin clearly enriched in the furrow (Figure 3B). A trend toward higher enrichment was observed in *ani-1(RNAi)* embryos, but the average (1.81 ± 0.12) was not statistically significant from wild type. However, *let-99(RNAi)* embryos exhibited a statistically significant decrease in myosin enrichment, to 1.38 ± 0.051. We also examined the effect of loss of ANI-1 and LET-99 on myosin enrichment in *zen-4(ts)* embryos. In *zen-4(ts)* embryos, we found a reduction in the level of myosin in the furrow compared with controls, consistent with previous reports (Canman *et al.*, 2008; Tse *et al.*, 2012). Although there was no difference in myosin levels in *ani-1(RNAi); zen-4 (ts)* embryos relative to *zen-4 (ts)* embryos, we did observe a statistically significant decrease in *let-99(RNAi);zen-4(ts)* embryos.

As another measurement of myosin localization, we also examined the distribution of myosin along the AP axis (Supplemental Figure S3). In *let-99(RNAi)* embryos, although the enrichment of myosin was less, myosin still accumulated at the furrow at higher levels than in regions of the cortex outside of the furrow (Supplemental Figure S3, A and B). However, in *let-99(RNAi);zen-4(ts)* embryos, accumulation of myosin was greatly reduced, and myosin failed to accumulate where the furrow would normally be (Supplemental Figure S3B). Even though there were no large myosin patches as previously reported for *ani-1(RNAi)* embryos (Maddox *et al.*, 2005), we observed no change in the distribution of myosin enrichment along the AP axis in either *ani-1(RNAi)* or *ani-1(RNAi);zen-4(ts)* embryos (Supplemental Figure S3B). Taken together with previous analyses of myosin patches (Maddox *et al.*, 2005; Werner *et al.*, 2007), these results demonstrate that LET-99 and ANI-1 have different effects on the localization and enrichment of myosin to the contractile ring, providing further evidence that they act in parallel mechanisms to promote furrow ingression.

FIGURE 3: LET-99 acts in the NOP-1 pathway and parallel to anillin. (A) Quantification of average furrow ingression in the genotypes listed. ns = *p* ≥ 0.05; *p < 0.05; **p < 0.01; ***p < 0.001; ****p < 0.0001. Error bars represent ± SEM. In addition to those labeled, all *zen-4* combinations are statistically different from control (*p* < 0.0001) and all double-mutant combinations with *zen-4(RNAi)* are statistically different than *zen-4* single mutants (*p* < 0.0001). (B) Top, representative image of an embryo expressing the NMY-2::mKate2 transgene at 100 s after anaphase onset. Bottom, schematic showing the regions of the embryo cortex that were measured; dashed line represents the area used to obtain values of the contractile ring signal, or where the contractile ring would otherwise be in genotypes that fail to furrow, and solid line represents the area used to obtain the cortical values outside of the contractile ring for normalization. (C) Quantification of NMY-2::mKate2 in the contractile ring in the listed genotypes. All genotypes are statistically different from control except for *ani-1(RNAi)*, *p* = 0.11.

Astral and central spindle microtubules are each sufficient to localize LET-99 at anaphase

Previous studies demonstrated that moving the mitotic spindle caused a concomitant shift in the position of the LET-99 band at anaphase (Bringmann et al., 2007), but whether astral microtubules or central spindle microtubules are required for LET-99 localization was not examined. We first tested whether astral microtubules are sufficient to localize LET-99 by examining YFP::LET-99 in zyg-9(RNAi) embryos, in which the small posterior spindle induces an astral microtubule–dependent anterior furrow (Werner et al., 2007; Loria et al., 2012; Supplemental Figure S2C). In these embryos, YFP::LET-99 initially localized in a posterior-lateral band at a position comparable to embryos with a normal bipolar spindle. However, before furrowing onset, YFP::LET-99 moved more anteriorly and marked the presumptive anterior cleavage furrow (nine of nine embryos). In a subset of zyg-9 embryos, we noticed a slight, transient increase in YFP::LET-99 signal in the posterior midzone-dependent furrow before posterior furrow ingression, in addition to the anterior furrow localization (n = 5 of 9; Supplemental Figure S2C). These observations suggest that astral microtubules are sufficient to localize LET-99 but also suggest that LET-99 localization may respond to the central spindle.

To test more rigorously which population of microtubules is required for LET-99 localization, we imaged YFP::LET-99 in both wild-type and par-3(it71) mutant backgrounds. Because LET-99 is uniformly cortical in prophase par-3(it71) embryos, this allowed for assessment of anaphase band localization specifically (Tsou et al., 2002). To quantify localization, we again traced the embryo cortex from anterior to posterior (0–100% EL) and divided the pixel intensities by the average cytoplasmic signal to generate a relative cortical/cytoplasmic enrichment. The individual embryo traces were then averaged to generate a line scan for each genotype (Figure 4; measurements of band width are given in Supplemental Table S1). To make quantitative comparisons, peak pixel intensities from each individual embryo trace were also obtained and averaged by genotype (Supplemental Table S2). In control embryos at NEB, a peak in pixel intensity of YFP::LET-99 (1.47 ± 0.017) was observed in the lateral posterior region, and the intensity of the peak increased at anaphase (1.89 ± 0.031; Figure 4, A and B, and Supplemental Tables S1 and S2). Consistent with previous antibody staining of par-3 embryos, there was uniform cortical localization of YFP::LET-99 at NEB, but by anaphase, a weak band was visible (peak value 1.38 ± 0.018) that was more centrally positioned (Figure 4 and Supplemental Tables S1 and S2).

We first addressed whether central spindle microtubules are required for LET-99 localization by depleting ZEN-4 via RNAi. zen-4(RNAi) embryos exhibited formation of the YFP::LET-99 band by NEB (intensity of 1.39 ± 0.021), and this band increased by anaphase (1.54 ± 0.030), although not to the same levels as in wild type (Figure 4A and Supplemental Table S1). In par-3(it71);zen-4(RNAi) embryos, a uniform cortical localization of YFP::LET-99 was present at NEB as expected. However, YFP::LET-99 became enriched in a band by the time of late anaphase with a peak intensity of 1.45 ± 0.022 (Figure 4A). Although this is lower than in wild type, it is not lower than for par-3(it71) alone. We conclude that centralspindlin/central spindle microtubules are not required for YFP::LET-99 localization at anaphase in the par-3–independent pathway.

Because our double- and triple-mutant analyses revealed that LET-99 acts in the NOP-1 pathway in parallel to ANI-1, we next tested whether either of these components is required for LET-99 localization. At NEB in nop-1(it142) embryos, YFP::LET-99 localized in a band with a peak of 1.32 ± 0.019. The band in nop-1 embryos was weaker in intensity and more posterior at NEB compared with wild type. Nonetheless, by anaphase, the band became more normally positioned and increased in intensity to 1.43 ± 0.022 (Figure 4A and Supplemental Tables S1 and S2). In ani-1(RNAi) embryos, peaks of 1.46 ± 0.036 and 1.46 ± 0.028 were observed at NEB and anaphase, respectively (Figure 4A and Supplemental Tables S1 and S2). The peaks at anaphase for both nop-1 and ani-1 embryos were significantly lower than in anaphase of wild type, but at least in the case of nop-1, the peak could be influenced by earlier polarity defects (Tse et al., 2012). Thus, to look specifically at anaphase LET-99 localization, we again used the par-3(it71) background. Quantification of nop-1(RNAi);par-3(it71) at late anaphase showed the formation of a centrally located LET-99 band with a peak intensity of 1.37 ± 0.021 (Figure 4 and Supplemental Tables S1 and S2). Similarly, we found that in ani-1(RNAi);par-3(it71) embryos, YFP::LET-99 was uniform at NEB but became enriched in a band with a peak intensity of 1.35 ± 0.028 (Figure 4A and Supplemental Tables S1 and S2). The levels at anaphase in both nop-1(RNAi);par-3(it71) and ani-1(RNAi);par-3(it71) embryos were not significantly different than in par-3(it71) embryos. Therefore we conclude that NOP-1 and ANI-1 are not required for the formation of the anaphase LET-99 band in par-3 embryos.

As described, in five of nine embryos with posterior spindles, we observed a transient enrichment of LET-99 in the posterior furrow, and this raised the possibility that either the centralspindlin or the astral pathway may be sufficient for LET-99 localization. To test this possibility, we examined YFP::LET-99 localization in par-3(it71);nop-1(RNAi);zen-4(RNAi) embryos. Quantification of YFP::LET-99 in these embryos showed uniform LET-99 signal at the cortex even in late anaphase (Figure 4, A and B). From these experiments, we conclude that either the centralspindlin or astral pathway is sufficient to localize LET-99 to the presumptive furrow.

LET-99 enrichment at the furrow is myosin dependent

Because both the centralspindlin and astral pathways appear sufficient to localize LET-99, and these pathways converge on RhoA, we hypothesized that LET-99 responds to RhoA and subsequent myosin activation (Tse et al., 2012). In addition to the population of myosin that comprises the contractile ring, myosin has also been observed to flow from the posterior cortex before furrow formation (Werner et al., 2007), and Gα and GPR-1/2 have been proposed to affect myosin flow via their effect on spindle elongation and spindle position (Werner et al., 2007; Schenk et al., 2010). Together with the failure of LET-99 to align with the furrow in Gα(RNAi) embryos, these findings raised the possibility that LET-99 is moved by myosin flow.

As noted earlier, when observed from a lateral view, the peak of the LET-99 can shift between NEB and anaphase, with the final position aligning with the furrow. To examine LET-99 more closely, we imaged YFP::LET-99 from a cortical view and generated a kymograph of a selected region of the cortex to detect any potential cortical movement (Figure 5A). This analysis revealed a narrowing of the region of highest intensity during anaphase and then a shift in the peak intensity before furrowing onset (eight of nine embryos). In strains expressing both YFP::LET-99 and NMY-2::mKate2, kymograph analysis showed that the shift of YFP::LET-99 occurred concomitant with myosin movement from the posterior toward the cleavage furrow (n = 8).

We next asked whether myosin is required for LET-99 localization to the equator and subsequent cleavage furrow. To address this question, we reduced the levels of NMY-2 protein via nmy-2(RNAi) and examined YFP::LET-99. Strong depletion of NMY-2 results in failures of both polarity establishment and cytokinesis
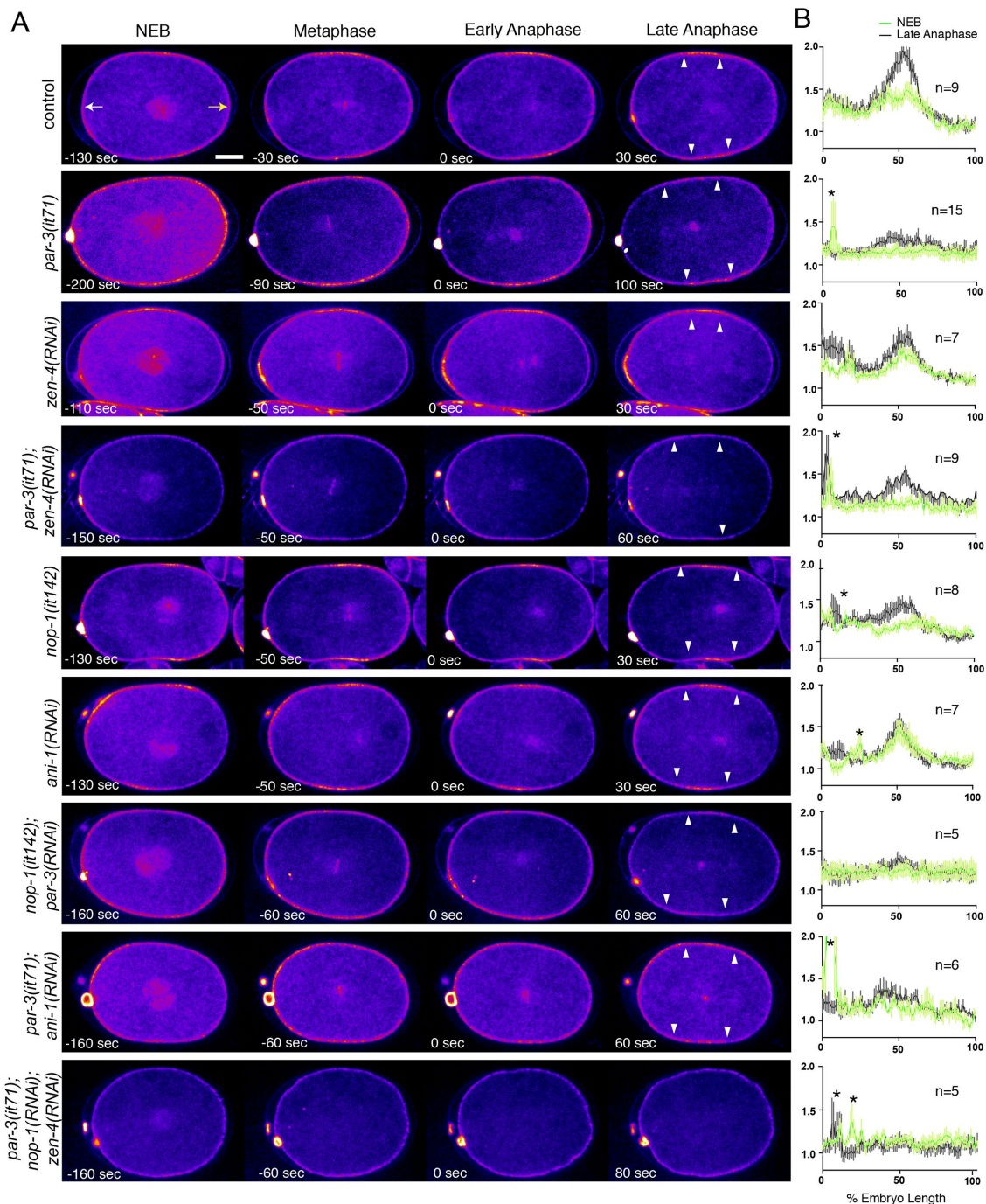
FIGURE 4: Either astral or central spindle microtubules are sufficient to localize LET-99 at anaphase. (A) Spinning-disk confocal images from time-lapse imaging of YFP::LET-99 transgenic embryos in the labeled backgrounds. Images are pseudocolored with Fire LUT such that the highest pixel values are pink/white and the lowest pixel values are blue/purple. Time relative to anaphase onset is shown in seconds. To generate a plot of intensity from anterior to posterior, both sides of the embryo cortex were traced from anterior (white arrow) to posterior (yellow arrow); arrowheads mark the LET-99 band as determined by the width of the peak of intensity at half-maximum. Scale bars represent 10 μm. (B) Average line scans for all embryos of a given genotype at NEB and late anaphase are shown with an asterisk marking peaks in signal from the polar body. Each graph corresponds to the genotype in the same row; *n* = number of embryos. Error bars represent ± SEM. See the text and Tables S1 and S2 for quantification of peak intensities and band position.

(Guo and Kemphues, 1996). We first imaged embryos at a mid focal plane and found that in embryos strongly depleted of NMY-2, a band of LET-99 did not form by the normal time of furrowing onset, and these embryos failed to divide (*n* = 8; Figure 5B). We also filmed YFP::LET-99; *nmy-2(RNAi)* embryos at a cortical plane

to investigate LET-99 movement. After long RNAi treatment, which resulted in a complete failure of cytokinesis, YFP::LET-99 was not assembled into a cortical band by NEB. However, unlike the case in *par-3* embryos, a LET-99 band did not form at anaphase in these *nmy-2(RNAi)* embryos (*n* = 8; Figure 5C). Under weaker RNAi
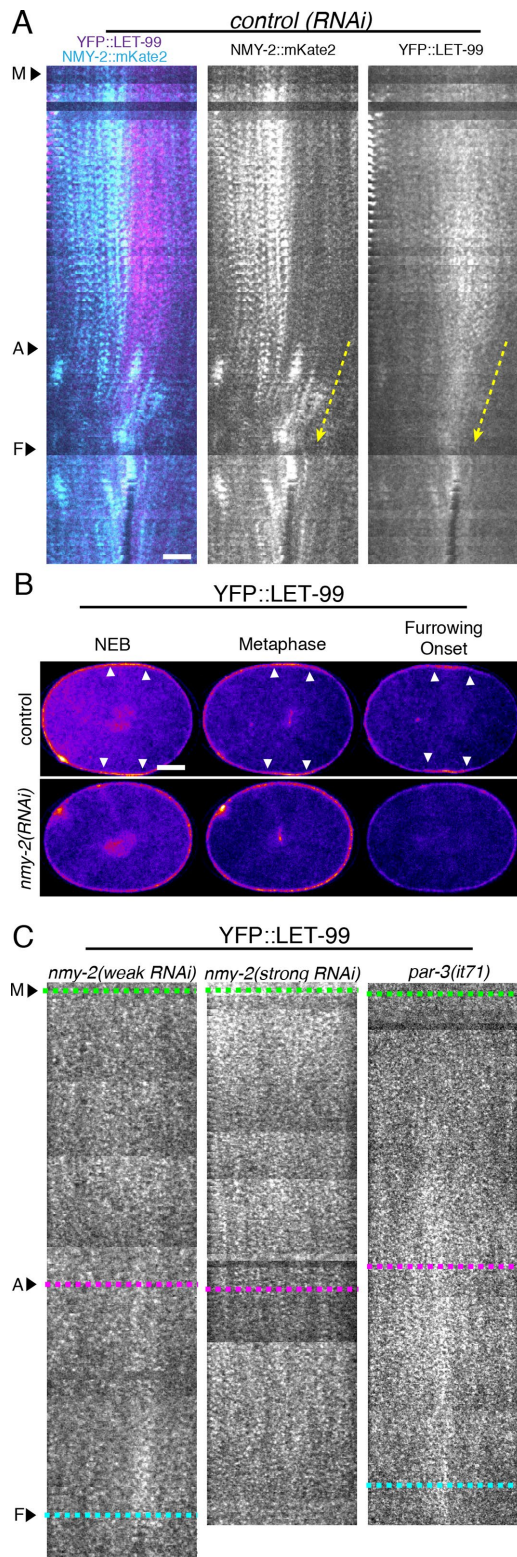
FIGURE 5: LET-99 localization is myosin dependent. (A) Kymograph of cortical images of YFP::LET-99 and NMY-2::mKate2 in the same embryo. Time is shown on the *y*-axis with 9 s between frames; M, A, and F represent metaphase, anaphase, and furrowing onset, respectively. Scale bar, 10 μm. Yellow arrows mark concomitant movement of NMY-2::mKate2 and YFP::LET-99 toward the furrow. (B) Stills from time-lapse fluorescence microscopy of YFP::LET-99 in control and strong depletion of NMY-2 by RNAi. Images are pseudocolored with Fire LUT such that the highest pixel values are

pink/white and the lowest pixel values are blue/purple. Arrowheads mark the band in control embryos. (C) Cortical kymograph of YFP::LET-99 in either *nmy-2(RNAi)* or *par-3(it71)* embryos. Colored lines represent metaphase, anaphase, or furrowing onset in green, magenta, and cyan, respectively.

conditions in which myosin knockdown resulted in failed pseudo-cleavage but not failed division, LET-99 became enriched at the presumptive cleavage furrow immediately before furrow initiation (*n* = 9; Figure 5C).

We therefore examined *par-3(it71)* embryos to see whether we could detect movement of YFP::LET-99 from both poles towards the equator. Although enrichment from cortical views was evident as expected, we did not detect obvious movement of LET-99, possibly due to the small size of LET-99 punctae. Taken together, these results suggest that NMY-2 is required for LET-99 localization to the presumptive cleavage furrow, but it remains unclear whether myosin flow is responsible for LET-99 localization.

DISCUSSION

In this article, we demonstrated a direct role for LET-99 in the aster-directed furrowing pathway during both asymmetric and symmetric cell division. We observed a dramatically reduced yet quantifiable furrow ingression in a majority of *let-99;centralspindlin* mutant embryos. Previous studies using either *zen-4* or laser ablation to remove the central spindle reported a greater number of embryos with a complete loss of furrowing (Bringmann *et al.*, 2007; Pacquelet *et al.*, 2015). The differences could be due to slight variations in the methods used to remove the central spindle or *zen-4* function. However, the effects are unlikely due to variability in spindle pole separation or spindle position, as our analysis of the extent of furrow ingression with these other defects failed to detect a correlation. Moreover, we found that LET-99 also functions in the symmetric division of the AB cell, where LET-99 is not required for nuclear rotation or anaphase spindle elongation. Together with the observed enrichment of LET-99 into a band before furrowing onset in the AB cell, these observations indicate that the role of LET-99 in cytokinesis is not coupled to its function in asymmetric spindle positioning.

Our observation that AB spindle elongation is less sensitive to loss of LET-99 prompted us to examine the effect of other components suggested to act in the aster-directed furrowing pathway. We found that *goa-1;gpa-16* RNAi-depleted embryos exhibited both normal spindle elongation and normal furrow ingression in a *central-spindlin*-minus background in the symmetrically dividing AB cell. Similarly, the AB cell in *gpb-1(RNAi);zen-4(ts)* embryos did not have stronger furrowing defects than *zen-4* mutants despite having high levels of GPR-1/2 similar to those seen in *let-99* mutants. Thus, whereas during spindle positioning and elongation LET-99 inhibits force generation via regulation of the G protein signaling pathway, LET-99 does not appear to function with Gα or Gβ for cytokinesis. Instead our results and studies of myosin flow in *Gα(RNAi)* and *gpr-1/2(RNAi)* embryos (Werner *et al.*, 2007; Schenk *et al.*, 2010) are most consistent with the model that the requirement for GOA-1/GPA-16 and GPR-1/2 in cytokinesis in the one-cell embryo is via their roles in spindle positioning and elongation, which acts to align the localization of the LET-99 band and potentially other molecules to the furrow.

We found that astral microtubules are sufficient to localize LET-99, consistent with the placement of LET-99 in the astral pathway.

Surprisingly, however, complete loss of LET-99 anaphase band localization was seen only when signals from both furrowing pathways were removed. This result suggests that both central spindle and astral microtubules localize LET-99 and is consistent with the presence of LET-99 at both the aster-positioned furrow and midzone-positioned furrow in situations in which the two furrows are separated (Figure 4C; Bringmann *et al.*, 2007). We also observed shifts in the localization of LET-99 at anaphase onset to match the furrow position, and these shifts were dependent on myosin activity. One possible model to explain the requirement of myosin activity for LET-99 localization is cortical myosin flow. Myosin flow is known to affect the localization of cortical components, most notably during polarity establishment in the *C. elegans* one-cell embryo. During polarity establishment, contractility of the cortical actomyosin network and subsequent anterior flow result in the simultaneous localization of anterior PAR polarity proteins by passive advective flow (Munro *et al.*, 2004). Myosin flows are also present during the maintenance phase of polarity, where anterior-directed myosin flow maintains active CDC-42 in the anterior through metaphase, and PAR-2 is required to prevent posterior directed flows that might otherwise result in mislocalization of PAR-3/PAR-6/PKC-3 during maintenance (Munro *et al.*, 2004; Beatty *et al.*, 2010). In addition, another period of myosin flow occurs after anaphase onset that results in bulk movements of myosin toward the cytokinesis furrow (Werner *et al.*, 2007). These cortical myosin flows never move through the furrow but accumulate with the furrow acting as a sink for myosin. The latter flows are proposed to facilitate not only cytokinesis but also "polarity correction," such that the border of the posterior PAR-2 domain is refined so that it coincides precisely with the cleavage furrow (Schenk *et al.*, 2010). PAR-2 polarity correction is dependent on Gα in embryos with a bipolar spindle but occurs normally in embryos with a posterior aster or spindle. We similarly found that Gα is required for alignment of the LET-99 band with the cleavage furrow in the one-cell embryo but not in the AB cell. Therefore we hypothesize that LET-99 localizes in response to cortical flows, and that Gα is required for such flows in the one-cell embryo due to its role in spindle elongation and positioning. Although myosin flow can explain the spindle-dependent localization of LET-99, we observed clear cortical movement of LET-99 foci only in control embryos (Figure 5A) and not in *par-3* embryos (Figure 5C). This may be a limitation of our acquisition times or the smallness of LET-99 punctae. Alternatively, LET-99 localization may depend on other myosin-dependent processes.

Our double- and triple mutant analyses of *let-99* and other astral furrowing components suggests that LET-99 acts in the same pathway as NOP-1, but that LET-99 acts in a parallel mechanism to ANI-1 during cytokinesis. It has been suggested that ANI-1 functions downstream of both NOP-1 and the centralspindlin complex, as ANI-1 fails to localize to the presumptive furrow in *nop-1;zen-4* and *nop-1;cyk-4* embryos (Tse *et al.*, 2012). Similarly, we observed that LET-99 also fails to localize to the cortex at the presumptive furrow in *par-3;nop-1;zen-4* embryos. Thus, although both LET-99 and ANI-1 appear to be downstream of both centralspindlin and astral pathways in terms of localization, the astral pathway is more sensitive to loss of either ANI-1 or LET-99. On the basis of these findings, we speculate that, similar to anillin, LET-99 may play a scaffolding role for components of the contractile ring that improves the robustness of cytokinesis. In support of this, we observed a decrease in the enrichment of myosin in the contractile ring upon depletion of LET-99 via RNAi. Furthermore, *let-99* mutants have disorganized cytokinetic rings

(Bringmann *et al.*, 2007). Motif searches of LET-99 and its orthologues reveal a region with partial homology to RhoGAP-like domains. The domain is degenerate, and thus LET-99 is not predicted to act as a GAP for RhoA. Nonetheless, LET-99 could potentially bind RhoA through this domain and serve as a docking site or scaffold for RhoA and other proteins required during cytokinesis.

In conclusion, we have shown that LET-99 acts in the aster-directed cytokinesis pathway of *C. elegans*, by a mechanism that is distinct from previously described roles for LET-99 during spindle positioning. We hypothesize that LET-99 promotes furrowing via a feedback mechanism in which a myosin-dependent process refines the cortical localization of LET-99 between the astral microtubules, and LET-99 then promotes the further enrichment of myosin, and possibly other contractile ring components, to the cleavage furrow. Future studies will determine the molecular mechanism by which LET-99 promotes myosin accumulation and furrowing.

MATERIALS AND METHODS

C. *elegans* strains

C. elegans strains were maintained on MYOB plates with *Escherichia coli* OP50 as a food source (Brenner, 1974; Church *et al.*, 1995). The following strains were used: TH73, ddIs64 [p*pie-1::yfp::let-99; unc-119(+)*] (Bringmann *et al.*, 2007); RL175, *let-99(dd17);unc-22(e66)/nT1*; KK820, *dpy-17 (e164) nop-1 (it142)* III (Rose and Kemphues, 1995); EU554, *zen-4(or153ts)* IV (Severson *et al.*, 2000); DH244, *zyg-9(b244ts)* II (Kemphues *et al.*, 1986); KK653, *par-3(it71); unc-32(e189)/qc1* III (Etemad-Moghadam *et al.*, 1995); LP229, p*nmy-2::nmy-2::mKate2* I. TH73 was crossed into RL175 to create RL238, and RL238 was crossed into KK653, LP229, and KK820 to create RL315, RL316, and RL337, respectively, for this study: RL238, ddIs64 [p*pie-1::yfp::let-99; unc-119(+)*]; *unc-22(e66) let-99 (dd17)* IV; RL315, ddIs64 [p*pie-1::yfp::let-99; unc-119(+)*]; *unc-22(e66) let-99 (dd17)* IV; *par-3 (it71)/qC1* III; RL316, ddIs64 [p*pie-1::yfp::let-99; unc-119(+)*]; *unc-22(e66) let-99 (dd17)* IV; p*nmy-2::nmy-2::mKate2* I; RL337, ddIs64 [p*pie-1::yfp::let-99; unc-119(+)*]; *unc-22(e66) let-99 (dd17)* IV; *nop-1(it142)* III); and RL349, p*nmy-2::nmy-2::mKate2* I; *zen-4(or153ts)* IV.

RNAi and mutant analysis

RNAi was performed by feeding (Timmons *et al.*, 2001). Unless otherwise noted, constructs used to induce RNAi were obtained from the Ahringer RNAi library (Kamath *et al.*, 2003) and include *ani-1 (III-6E18)*, *goa-1 (I-3P15)*, *gpb-1 (II-8A05)*, *let-99 (IV-6P07)*, *nop-1 (III-3K05)*, *nmy-2 (I-3L24)*, *par-3 (III-3A01)*, *zen-4 (IV-3107)*, and *zyg-9 (II-6M11)*. The *gpa-16* clone was from Park and Rose (2008). The full-length *zyg-1* template was PCR-amplified from F59E12.2 cDNA and included an *Eco*RI recognition sequence for ligation into pL4440. For double RNAi feeding experiments, bacteria cultures were mixed equally according to cell density (OD_{600}). The extent of RNAi efficiency was determined by the observance of known phenotypes for each construct as follows. 1) *zen-4*: increased pole-to-pole distance of the anaphase spindle and loss of central spindle microtubules. 2) *let-99*: severe nuclear-centrosome rocking and failure of P1 nuclear rotation. 3) *zyg-9*: the presence of a small posterior spindle. 4) ANI-1 and NOP-1 depletions were scored based on the lack of pseudocleavage, as well as either large or absent polar bodies for *ani-1(RNAi)*. 5) To determine the extent of depletion in *goa-1/gpa-16* embryos, we scored embryos for defects in centration and P1 spindle rotation failure. 6) Strong PAR-3 depletion was assessed by the absence of LET-99 band localization at NEB,

which was used as a proxy for loss of polarity; presence of a centrally located anaphase spindle; and a symmetric cell division. 7) Strong depletion of NMY-2 was assessed by failure to localize LET-99 in a band at NEB and failure to furrow. 8) Finally, ZYG-1 depletion was determined by the presence of a monopolar spindle in the AB and P1 blastomeres.

Time-lapse microscopy

Worms were dissected in egg buffer (25 mM 4-(2-hydroxyethyl)-1-piperazineethanesulfonic acid, pH 7.4, 120 mM NaCl, 48 mM KCl, 2 mM CaCl$_2$, MgCl$_2$), and embryos were mounted on 2% agarose pads in the same buffer. To score furrow ingression, differential interference contrast (DIC) or bright-field images of live embryos were captured using an Olympus BX60 compound microscope using a PlanApo N 60×/1.42 numerical aperture (NA) oil-immersion objective, Hamamatsu Orca 12-bit digital camera, and OpenLab software (Improvision/PerkinElmer, Waltham MA) or Micromanager (Edelstein *et al.*, 2001). Single-plane images were acquired every 10 s. Temperature shifts were performed using a Linkam PE95/T95 System Controller with EP Water Circulation Pump (Linkam Scientific Instruments, Tadworth, United Kingdom), and the actual slide temperature was determined using an Omega HH81 digital thermometer as in Liro and Rose (2016). For *zen-4(ts)*, embryos were mounted and incubated at 16°C until NEB, when the embryos were shifted to the nonpermissive temperature (26°C).

Short time-lapse experiments of YFP::LET-99 and NMY-2::mKate2 expressing embryos were performed using the spinning-disk module of a Marianas SDC Real-Time 3D Confocal-TIRF microscope (Intelligent Imaging Innovations) fit with a Yokogawa spinning-disk head, a 63×/1.3 NA oil-immersion objective, and electron-multiplying charge-coupled device camera. Acquisition was controlled by SlideBook 6 software (3i Incorporated). For spinning-disk imaging, single focal planes are shown and were acquired every 10 s for cross-section and every 3 s for cortical views. All raw images were exposed and scaled with the same parameters.

Data analysis

The extent of furrowing was measured from bright-field and DIC images as described in the text. For spindle pole elongation, the distance between the center of the anterior and posterior spindle poles was measured at the frame before furrowing onset. The distance is reported as a percentage of embryo length (the distance measured relative to the length of the embryo) as well as the absolute spindle length reported in micrometers. Times given relative to NEB were determined by spindle pole movement, chromosome splitting, and/or elapsed time relative to NEB for each strain. Measurements were exported into Excel or Prism (GraphPad Software) for further analysis. Unpaired two-tailed *t* tests and Pearson (normally distributed data) and Spearman (nonnormally distributed data) correlations were conducted in Prism.

YFP localization in one-cell embryos was measured at NEB and late anaphase (frame before furrowing onset). Measurements of cortical pixel intensities of YFP::LET-99 were made using the segmented line tool in Fiji (Schindelin *et al.*, 2012) and normalized to the signal of the adjacent cytoplasm. Measurements were exported into Excel or Prism for further analysis. To control for differences in pixel number across the embryos of different lengths, the number of pixels was converted to percentage egg length (% EL) by combining the pixel values into 1% bins from 0 to 100% and reported as a function of EL. The highest

intensity pixels (excluding the polar body signal) were used to identify the apex of the LET-99 band, and then values from a window of ±5% on either side of this were averaged to determine the peak pixel intensity for each individual embryo. For NEB in *par-3* backgrounds, where there was no band, the window was centered on 50% EL. To create average line scans for each genotype in the results, individual traces were averaged. From these graphs, the full-width at half-maximum was obtained by identifying the values that correspond to half of the maximum peak value on either side of the peak. Graphs were generated in GraphPad Prism using the exported data. Unpaired two-tail *t* tests were performed in Prism.

To assess cortical movements of NMY-2 and LET-99, kymographs of NMY-2::mKate2 and YFP::LET-99 were generated using the montage tool in Fiji. The kymographs represent regions of the cortex picked manually and with each frame representing the chosen region of the cortex every 3 s.

To assess changes in YFP::LET-99 localization in *zyg-1(RNAi)* two-cell embryos, measurements of cortical pixel intensities were made using the segmented line tool in Fiji at NEB and late anaphase and normalized to the signal of the adjacent cytoplasm as before. The number of pixels was normalized by 1% binning from 0 to 100% of the AB cortex as shown in the figure. The fold difference between NEB and late anaphase pixel intensities from 0 to 100% was calculated for each embryo, and values for each embryo were then averaged to generate an average line scan of the AB cortex.

To measure myosin enrichment, alternating cortical midfocal images of NMY-2::mKate2 were obtained every 3 s at 100-ms exposure. Mean pixel intensity values corresponding to a 20-pixel by 60-pixel region of interest in the furrow were obtained and normalized to the cytoplasmic signal on the posterior side of the contractile ring. Measurements were taken at 100 s after anaphase, as this time point allows quantification of contractile ring enrichment before the furrow regressed in all but *let-99(RNAi);zen-4(ts)* and *ani-1(RNAi);let-99(RNAi);zen-4(ts)* embryos. Because these embryos sometimes failed to furrow, cortical signal was measured by placing the region of interest between the anaphase chromosomes as determined from the midfocal image at that same time point.

REFERENCES

Adams RR, Tavares AAM, Salzberg A, Bellen HJ, Glover DM (1998). *Pavarotti* encodes a kinesin-like protein required to organize the central spindle and contractile ring for cytokinesis. Genes Dev 12, 1483–1494.

Afshar K, Willard FS, Colombo K, Johnston CA, McCudden CR, Siderovski DP, Gönczy P (2008). RIC-8 Is required for GPR-1/2-dependent; function during asymmetric division of C. elegans embryos. Cell 119, 219–230.

Alsop GB, Zhang D (2004). Microtubules continuously dictate distribution of actin filaments and positioning of cell cleavage in grasshopper spermatocytes. J Cell Sci 117, 1591–1602.

Basant A, Lekomtsev S, Tse YC, Zhang D, Longhini KM, Petronczki M, Glotzer M (2015). Aurora B kinase promotes cytokinesis by inducing centralspindlin oligomers that associate with the plasma membrane. Dev Cell 33, 204–215.

Beatty A, Morton D, Kemphues K (2010). The C. elegans homolog of Drosophila Lethal giant larvae functions redundantly with PAR-2 to maintain polarity in the early embryo. Development 137, 3995.

Brenner S (1974). The genetics of Caenorhabditis elegans. Genetics 77, 71.

Bringmann H, Cowan CR, Kong J, Hyman AA (2007). LET-99, GOA-1/GPA-16, and GPR-1/2 are required for aster-positioned cytokinesis. Curr Biol 17, 185–191.

Bringmann H, Hyman AA (2005). A cytokinesis furrow is positioned by two consecutive signals. Nature 436, 731–734.

Canman JC, Lewellyn L, Laband K, Smerdon SJ, Desai A, Bowerman B, Oegema K (2008). Inhibition of Rac by the GAP activity of centralspindlin is essential for cytokinesis. Science 322, 1543–1546.

Cao LG, Wang YL (1996). Signals from the spindle midzone are required for the stimulation of cytokinesis in cultured epithelial cells. Mol Biol Cell 7, 225–232.

Carvalho A, Desai A, Oegema K (2009). Structural memory in the contractile ring makes the duration of cytokinesis independent of cell size. Cell 137, 926–937.

Chen W, Foss M, Tseng K-F, Zhang D (2008). Redundant mechanisms recruit actin into the contractile ring in silkworm spermatocytes. PLoS Biol 6, e209.

Church DL, Guan KL, Lambie EJ (1995). Three genes of the MAP kinase cascade, mek-2, mpk-1/sur-1 and let-60 ras, are required for meiotic cell cycle progression in Caenorhabditis elegans. Development 121, 2525.

D'Avino PP, Savoian MS, Glover DM (2005). Cleavage furrow formation and ingression during animal cytokinesis: a microtubule legacy. J Cell Sci 118, 1549–1558.

Dechant R, Glotzer M (2003). Centrosome separation and central spindle assembly act in redundant pathways that regulate microtubule density and trigger cleavage furrow formation. Dev Cell 4, 333–344.

Edelstein A, Amodaj N, Hoover K, Vale R, Stuurman N (2001). Computer control of microscopes using μManager. Curr Protoc Mol Biol Chapter 14, Unit 14.20.

Eggert US, Mitchison TJ, Field CM (2006). Animal cytokinesis: from parts list to mechanisms. Annu Rev Biochem 75, 543–566.

Etemad-Moghadam B, Guo S, Kemphues KJ (1995). Asymmetrically distributed PAR-3 protein contributes to cell polarity and spindle alignment in early *C. elegans* embryos. Cell 83, 743–752.

Foe VE, von Dassow G (2008). Stable and dynamic microtubules coordinately shape the myosin activation zone during cytokinetic furrow formation. J Cell Biol 183, 457–470.

Glotzer M (2004). Cleavage furrow positioning. J Cell Biol 164, 347–351.

Glotzer M (2005). The molecular requirements for cytokinesis. Science 307, 1735–1739.

Green RA, Paluch E, Oegema K (2012). Cytokinesis in animal cells. Annu Rev Cell Dev Biol 28, 29–58.

Guo S, Kemphues KJ (1996). A non-muscle myosin required for embryonic polarity in Caenorhabditis elegans. Nature 382, 455–458.

Jantsch-Plunger V, Gönczy P, Romano A, Schnabel H, Hamill D, Schnabel R, Hyman AA, Glotzer M (2000). Cyk-4: a Rho family Gtpase activating protein (Gap) required for central spindle formation and cytokinesis. J Cell Biol 149, 1391–1404.

Jordan SN, Davies T, Zhuravlev Y, Dumont J, Shirasu-Hiza M, Canman JC (2016). Cortical PAR polarity proteins promote robust cytokinesis during asymmetric cell division. J Cell Biol 212, 39–49.

Kamath RS, Fraser AG, Dong Y, Poulin G, Durbin R, Gotta M, Kanapin A, Le Bot N, Moreno S, Sohrmann M, *et al.* (2003). Systematic functional analysis of the Caenorhabditis elegans genome using RNAi. Nature 421, 231–237.

Kemphues KJ, Wolf N, Wood WB, Hirsh D (1986). Two loci required for cytoplasmic organization in early embryos of *Caenorhabditis elegans*. Dev Biol 113, 449–460.

Krueger LE, Wu J-C, Tsou M-FB, Rose LS (2010). LET-99 inhibits lateral posterior pulling forces during asymmetric spindle elongation in *C. elegans* embryos. J Cell Biol 189, 481–495.

Lewellyn L, Dumont J, Desai A, Oegema K (2010). Analyzing the effects of delaying aster separation on furrow formation during cytokinesis in the Caenorhabditis elegans embryo. Mol Biol Cell 21, 50–62.

Liro MJ, Rose LS (2016). Mitotic spindle positioning in the EMS cell of Caenorhabditis elegans requires LET-99 and LIN-5/NuMA. Genetics 204, 1177–1189.

Loria A, Longhini KM, Glotzer M (2012). The RhoGAP domain of CYK-4 has an essential role in RhoA activation. Curr Biol 22, 213–219.

Maddox AS, Habermann B, Desai A, Oegema K (2005). Distinct roles for two *C. elegans* anillins in the gonad and early embryo. Development 132, 2837–2848.

Maddox AS, Oegema K (2003). Deconstructing cytokinesis. Nat Cell Biol 5, 773–776.

Morton DG, Hoose WA, Kemphues KJ (2012). A genome-wide RNAi Screen for enhancers of par mutants reveals new contributors to early embryonic polarity in Caenorhabditis elegans. Genetics 192, 929–942.

Munro E, Nance J, Priess JR (2004). Cortical flows powered by asymmetrical contraction transport PAR proteins to establish and maintain anterior-posterior polarity in the early *C. elegans* embryo. Dev Cell 7, 413–424.

Murthy K, Wadsworth P (2008). Dual role for microtubules in regulating cortical contractility during cytokinesis. J Cell Sci 121, 2350–2359.

O'Connell KF, Caron C, Kopish KR, Hurd DD, Kemphues KJ, Li Y, White JG (2001). The *C. elegans* zyg-1 gene encodes a regulator of centrosome duplication with distinct maternal and paternal roles in the embryo. Cell 105, 547–558.

Pacquelet A, Uhart P, Tassan J-P, Michaux G (2015). PAR-4 and anillin regulate myosin to coordinate spindle and furrow position during asymmetric division. J Cell Biol 210, 1085–1099.

Panbianco C, Weinkove D, Zanin E, Jones D, Divecha N, Gotta M, Ahringer J (2008). A casein kinase 1 and PAR proteins regulate asymmetry of a PIP2 synthesis enzyme for asymmetric spindle positioning. Dev Cell 15, 198–208.

Park DH, Rose LS (2008). Dynamic localization of LIN-5 and GPR-1/2 to cortical force generation domains during spindle positioning. Dev Biol 315, 42–54.

Pavicic-Kaltenbrunner V, Mishima M, Glotzer M (2007). Cooperative assembly of CYK-4/MgcRacGAP and ZEN-4/MKLP1 to form the centralspindlin complex. Mol Biol Cell 18, 4992–5003.

Piekny A, Werner M, Glotzer M (2005). Cytokinesis: welcome to the Rho zone. Trends Cell Biol 15, 651–658.

Piekny AJ, Glotzer M (2008). Anillin is a scaffold protein that links RhoA, actin, myosin during cytokinesis. Curr Biol 18, 30–36.

Piekny AJ, Maddox AS (2010). The myriad roles of anillin during cytokinesis. Semin Cell Dev Biol 21, 881–891.

Pollard TD (2010). Mechanics of cytokinesis in eukaryotes. Curr Opin Cell Biol 22, 50–56.

Raich WB, Moran AN, Rothman JH, Hardin J (1998). Cytokinesis and midzone microtubule organization in *Caenorhabditis elegans* require the kinesin-like protein ZEN-4. Mol Biol Cell 9, 2037–2049.

Rappaport R (1996). Cytokinesis in Animal Cells, Cambridge, UK: Cambridge University Press.

Rose L, Gonczy P (2014). Polarity establishment, asymmetric division and segregation of fate determinants in early *C. elegans* embryos. WormBook 2014(Dec 30), 1–43.

Rose LS, Kemphues K (1998). The *let-99* gene is required for proper spindle orientation during cleavage of the *C. elegans* embryo. Development 125, 1337–1346.

Rose LS, Lamb ML, Hird SN, Kemphues KJ (1995). Pseudocleavage is dispensable for polarity and development in *C. elegans* embryos. Dev Biol 168, 479–489.

Schenk C, Bringmann H, Hyman AA, Cowan CR (2010). Cortical domain correction repositions the polarity boundary to match the cytokinesis furrow in *C. elegans* embryos. Development 137, 1743–1753.

Schindelin J, Arganda-Carreras I, Frise E, Kaynig V, Longair M, Pietzsch T, Preibisch S, Rueden C, Saalfeld S, Schmid B, *et al.* (2012). Fiji—an open source platform for biological image analysis. Nat Methods 9, 10.1038/nmeth.2019.

Severson AF, Hamill DR, Carter JC, Schumacher J, Bowerman B (2000). The Aurora-related kinase AIR-2 recruits ZEN-4/CeMKLP1 to the mitotic spindle at metaphase and is required for cytokinesis. Curr Biol 10, 1162–1171.

Timmons L, Court DL, Fire A (2001). Ingestion of bacterially expressed dsRNAs can produce specific and potent genetic interference in *Caenorhabditis elegans*. Gene 263, 103–112.

Tse YC, Piekny A, Glotzer M (2011). Anillin promotes astral microtubule-directed cortical myosin polarization. Mol Biol Cell 22, 3165–3175.

Tse YC, Werner M, Longhini KM, Labbe J-C, Goldstein B, Glotzer M (2012). RhoA activation during polarization and cytokinesis of the early *Caenorhabditis elegans* embryo is differentially dependent on NOP-1 and CYK-4. Mol Biol Cell 23, 4020–4031.

Tsou M-FB, Hayashi A, DeBella LR, McGrath G, Rose LS (2002). LET-99 determines spindle position and is asymmetrically enriched in response to PAR polarity cues in *C. elegans* embryos. Development 129, 4469–4481.

Tsou M-FB, Hayashi A, Rose LS (2003). LET-99 opposes Gα/GPR signaling to generate asymmetry for spindle positioning in response to PAR and MES-1/SRC-1 signaling. Development 130, 5717–5730.

Verbrugghe KJC, White JG (2004). SPD-1 is required for the formation of the spindle midzone but is not essential for the completion of cytokinesis in *C. elegans* embryos. Curr Biol 14, 1755–1760.

von Dassow G (2009). Concurrent cues for cytokinetic furrow induction in animal cells. Trends Cell Biol 19, 165–173.

Werner M, Glotzer M (2008). Control of cortical contractility during cytokinesis. Biochem Soc Trans 36, 371–377.

Werner M, Munro E, Glotzer M (2007). Astral signals spatially bias cortical myosin recruitment to break symmetry and promote cytokinesis. Curr Biol 17, 1286–1297.

Wheatley SP, Wang Y (1996). Midzone microtubule bundles are continuously required for cytokinesis in cultured epithelial cells. J Cell Biol 135, 981–989.

Wu J-C, Espiritu EB, Rose LS (2016). The 14-3-3 protein PAR-5 regulates the asymmetric localization of the LET-99 spindle positioning protein. Dev Biol 412, 288–297.

Wu J-C, Rose LS (2007). PAR-3 and PAR-1 inhibit LET-99 localization to generate a cortical band important for spindle positioning in Caenorhabditis elegans embryos. Mol Biol Cell 18, 4470–4482.

Zhou M, Wang Y-L (2008). Distinct pathways for the early recruitment of myosin II and actin to the cytokinetic furrow. Mol Biol Cell 19, 318–326.

Zumdieck A, Kruse K, Bringmann H, Hyman AA, Jülicher F (2007). Stress generation and filament turnover during actin ring constriction. PLoS One 2, e696.